



Metal-confined synthesis of ZnS2 monolayer catalyst for dinitrogen electroreduction

R. Zhang, X. Tong

To be published in "ACS CATALYSIS"

June 2022

Center for Functional Nanomaterials

Brookhaven National Laboratory

U.S. Department of Energy

USDOE Office of Science (SC), Basic Energy Sciences (BES) (SC-22)

Notice: This manuscript has been authored by employees of Brookhaven Science Associates, LLC under Contract No.DE-SC0012704 with the U.S. Department of Energy. The publisher by accepting the manuscript for publication acknowledges that the United States Government retains a non-exclusive, paid-up, irrevocable, world-wide license to publish or reproduce the published form of this manuscript, or allow others to do so, for United States Government purposes.

DISCLAIMER

This report was prepared as an account of work sponsored by an agency of the United States Government. Neither the United States Government nor any agency thereof, nor any of their employees, nor any of their contractors, subcontractors, or their employees, makes any warranty, express or implied, or assumes any legal liability or responsibility for the accuracy, completeness, or any third party's use or the results of such use of any information, apparatus, product, or process disclosed, or represents that its use would not infringe privately owned rights. Reference herein to any specific commercial product, process, or service by trade name, trademark, manufacturer, or otherwise, does not necessarily constitute or imply its endorsement, recommendation, or favoring by the United States Government or any agency thereof or its contractors or subcontractors. The views and opinions of authors expressed herein do not necessarily state or reflect those of the United States Government or any agency thereof.

Metal-confined synthesis of ZnS₂ monolayer catalyst for dinitrogen electroreduction

Rui Zhang^{1,2}, Xiao-Hua Liu¹, De-Yao Wu¹, Hai-Bin Wang¹, Chuan-Qi Cheng¹, Qian-Jin Guo¹, Jing Mao^{1,6}, Tao Ling¹, Cun-Ku Dong¹, Hui Liu¹, Bo-Qun Zhang², Xue-Li Zheng³, Li-Li Han^{2,4}, Jing-Min Zhang⁵, Ashley Head⁶, Xiao Tong⁶, Zhixiu Liang⁷, Jun Luo^{4*}, Huolin L. Xin^{2*} and Xi-Wen Du^{1*}

1 Institute of New Energy Materials, School of Materials Science and Engineering, Tianjin University, Tianjin 300072, P. R. China.

- 2 Department of Physics and Astronomy, University of California, Irvine, CA 92697 USA.
- 3 Department of Material Science and Engineering, Stanford University, Stanford, CA 94305, USA.
- 4 Institute of New Energy Materials and Low-carbon Technologies, Tianjin University of Technology, Tianjin 300384, P. R. China.
- 5 Electron Microscopy Laboratory, School of Physics, Peking University, Beijing 100871, P. R. China

6 Center for Functional Nanomaterials, Brookhaven National Laboratory, Upton, NY, 11973, USA.

7 Department of Chemistry, Stony Brook University, Stony Brook, NY 11794, USA.

KEYWORDS. 2D Materials; Monolayer; Dichalcogenides; Nitrogen Reduction Reaction; N₂ adsorption.

ABSTRACT. Atomically thin two-dimensional (2D) materials are of great significance in catalyst, energy storage and electronic device. So far, such materials are limited to several categories with layered structure. Herein, we predict an unusual atomically thin ZnS₂ monolayer, and exploit a metal-confined chemical vapor deposition strategy for the successful preparation of such an unprecedented 2D material, where sulfide monolayer was firstly grown on metal nanosheets to form a sulfide/metal/sulfide sandwich structure, and then the metal core was etched out to obtain freestanding sulfide monolayers. The ZnS₂ monolayer possesses unique electron-deficient properties related to the atomic structure and exhibits high catalytic activity for dinitrogen electroreduction. Our work will enable creating 2D TMDs materials that were previously inexistent or inaccessible.

Introduction

Ultrathin two-dimensional (2D) nanomaterials, especially transition metal dichalcogenides (TMDs), emerge as attractive building blocks for catalytic^{1, 2}, photonic^{3, 4}, and electronic^{5, 6} systems due to their unique atomic/electronic structures and hundreds of configurations with the

change of metal species and chalcogenides. Particularly, TMDs show great potential in electrochemical catalysis such as hydrogen evolution reaction⁷ (HER) and N₂ reduction reaction⁸ (NRR). Conventional 2D TMDs such as MoS₂, though proved to be efficient in HER, shows very unsatisfied activity and selectivity in NRR owing to the weak adsorption of N₂ molecules⁸. The recent work shows that by tunning the transition metal species, the NRR selectivity of can be significantly improved⁹. Thus, exploring and expanding the boundaries of TMDs materials family are of great importance both experimentally and theoretically.

With concerted interests, the field has evolved rapidly in the past few decades^{10, 11}. Now, the TMDs family has been expanded from Mo/W-based dichalcogenides to binary, ternary, and even those of noble metals, such as PtS₂ and PtSe₂ (see Table S1)¹²⁻¹⁸. Notably, a universal approach based on molten-salt-assisted chemical vapor deposition has been developed and 47 kinds of atomically thin TMDs have been synthesized, involving nearly all transition metals¹⁹.

Although exciting progresses have been made over the past few years, 2D metal dichalcogenides with non-transition metal cations are still missing from the phase diagrams. The challenge lies in the fact that the bonds between non-transition metal and sulfur spread in three dimensions, and it is hard to form the layered structure spontaneously in those compounds, let alone exfoliating 2D flakes from their parent crystals. In addition, from the theoretical point of view, the highest oxidation state of non-transition metals is less than +3, making them incapable of providing four valence electrons to the two S²⁻ in dichalcogenides.

Zinc locates at the borderline of d-block metal in the periodic table, with fully occupied both d-and s-orbits (3d¹⁰4s²), thus it is generally excluded from the transition metals and more analogous to the alkaline earth metals in terms of the atomic radii, ionic radii, and electronegativities²⁰⁻²³. In

a conventional synthesis process, zinc sulfides are usually grown into nanoparticles²⁴ or nanowires²⁵ to minimize surface energy and/or accommodate the polarity of different termination, as indicated by Wulff construction theory²⁶. So far, 2D nanostructures have never been reported for the zinc sulfide.

Notably, the surface and interface effect can modify the crystal growth and the product morphology dramatically^{27, 28}. A typical example is the growth of graphene on copper surface, where metallic surface induces the 2D growth of carbon material²⁹. Inspired by this successful precedent, for the first time we managed to confine the growth of dichalcogenides on metal surface and obtained ZnS₂ monolayers on zinc core via a CVD technique. After the zinc core was etched out, the free-standing ZnS₂ monolayers were obtained and show a novel 1-T phase with sulfur anions in a reduced valance state (close to -1). The unique crystal and electronic structures of ZnS₂ monolayer cause enhanced chemical coupling, leading to high faradaic efficiency in electrochemical NRR.

Results and Discussion

To test the possibility of monolayer ZnS₂ materials, we first adopted ab-initio calculations to investigate the ground-state energy of three typical phases, including 1T, 1T' and 2H. As shown in Figure 1A and Table S2, 1-T phase ZnS₂ is more stable compared with 2-H and 1-T' ZnS₂ in the light of the more negative value of electronic energy. The phonon spectrum is also calculated, showing that monolayer 1-T ZnS₂ is stable in freestanding state (Figure S1). Despite the theoretical feasibility, the synthesis of such "unknown" material is a big challenge. The ab-initio calculation is conducted on the confined growth of ZnS₂ monolayers on Zn surface. The results indicate that ZnS₂ layer can be adsorbed tightly on Zn (0002) surface, with adsorption energy (Ead) of

~2.68eV/unit cell (Figure 1B and Figure S2). Once Zn surface is covered by ZnS₂ monolayer, the adsorption of ZnS₂ clusters is mostly prohibited due to the rapid attenuation of Ead to 0.26 eV. As such, a stable ZnS₂ monolayer can be obtained on the Zn surface.

Based on the theoretical prediction, a CVD technique was employed for the synthesis of ZnS₂ monolayers where Zn vapor directly reacts with S-contained gas (Figure 1C). Different sulfur sources (such as SO₂, S powder and CS₂) are investigated under the same synthetic conditions. As shown in Figures S3-S6, CS₂ was found to be the only sulfur source which can produce large amount of ultrathin nanosheets (with total thickness around 4 nm). The energy dispersive spectrometer (EDS) line profile, X-ray photoelectron spectrometer (XPS) and energy filtered transmission electron microscope (EFTEM) of a cross-section sample reveal a sandwich structure with ultrathin (<1 nm) Zn-S surface layer and pure Zn core layer (Figures S7-S9). The selected area electron diffraction (SAED) pattern in Figure S10 shows two sets of conformal patterns along [0002] zone axis of hexagonal phases, suggesting the coexistence of zinc single crystal (spots) and zinc sulfide (short arc). Furthermore, high angle annular dark field STEM (HAADF-STEM) observation of outermost surface indicates the unusual atomic structure which is analogous to the side view of the 1-T phase rather than the bulk ZnS phase (Figure S11). The above results demonstrate that atomically thin Zn-S layer with novel phase is obtained on metallic Zn surface.

In the next step, Zn core was eliminated by either heating to 673 K in ultrahigh vacuum (UHV) (< 10⁻⁵ Pa) or etched in 5 vol% acetic acid solution. The in-situ observation clearly shows the removal process of Zn core (Figures S12-S14) without phase change and damage of ZnS₂ structure. The obtained pure Zn-S layer displays large lateral size (>10 μm) and is transparent for the low energy secondary electrons in scanning electron microscope (Figure 2A), implying the ultrathin thickness. Indeed, the average thickness of Zn-S layer is determined as 0.66 nm by atomic force

microscope (AFM), corresponding to 2~3 atom layers (Figure S15). Moreover, the Zn-S layer presents an X-ray diffraction (XRD) pattern distinct from bulk ZnS, with a single broaden peak locating at ~29° (Figure 2B) which can be attributed to the (100) plane, this result suggests that only one type of continuous crystal plane exists in the Zn-S layer.

To further probe the structure of Zn-S monolayer, aberration-corrected high-resolution TEM and HAADF-STEM were employed to investigate the atomic arrangement in the plane and side views, respectively. In the plane view HADDF-STEM image (Figure 2C and Figure S16), Zn-S monolayer exhibits an atomic arrangement with 1-T phase structure, where the vacancy sites of wurtzite ZnS are occupied by a set of additional low contrast atoms. Since the contrast of HAADF-STEM image is sensitive to the projected atomic mass (known as Z-contrast), the Zn:S ratio is facilely estimated as 1:2 by counting the high contrast (zinc) and low contrast (sulfur) sites, according well with the results of XPS and EDS quantification (Figures S17-S19). The 1-T atomic structure is also verified by direct observation of cross-section specimen (Figure 2D and Figure S20). Moreover, HAADF-STEM and HRTEM images of various phase structures were simulated at the testing conditions (Figures S21-S23), it was found that only the monolayer ZnS2 with 1-T configuration matches well with the experiment results. Meanwhile, the UHV scanning tunneling microscopy (STM) was conducted to study the arrangement of outermost atoms. Figure 2E clearly shows the (0002) surface sulfur atoms with hexagonal structure and the sublayer Zn atoms with weaker intensity (after FFT filtered, Figure S24), presenting a structure analogical to 1-T MoS2³⁰.

Fourier transformed extended X-ray absorption fine structure (EXAFS) profile of Zn K-edge provides statistic information on the atomic structure of monolayer ZnS₂. As shown in Figure 2F, both ZnS₂ and bulk ZnS show intensive peaks from Zn-S scattering, while the intensity of Zn-Zn scattering attenuated sharply in ZnS₂ compared with bulk ZnS. More intriguingly, the Zn-Zn

scattering path out of (0002) plane vanishes, indicating that all of Zn atoms locate in (0002) plane, corresponding with the monolayer 1-T structure. Furthermore, compared with bulk ZnS, coordination number (CN) fitting (Figures S25-S27) shows the noticeable increase of Zn-S bond scattering in monolayer ZnS₂ which always signify the higher CN (ca. from ZnS bulk 2.8±0.28 to monolayer ZnS₂ 4.4±1.2). The difference of CNs originates from the change of phase structure, from tetrahedral coordination of Zn atoms in bulk ZnS to octahedral coordination in 1-T ZnS₂, leading to the number of nearest neighbor sulfur atoms increasing from 4 to 6. Based on the above analysis, we conclude that the monolayer ZnS₂ with 1-T structure is uniformly obtained in our experiment (Figure 2G).

XPS is adopted to detect the sulfur valence states of ZnS₂ monolayer. As shown in Figure 3A, the S peak of ZnS₂ (~162.4eV) locates between S⁰ of sulfur powder (~163.8eV) and S²⁻ of ZnS (~161.6eV), and close to the S₂²⁻ of pyrite FeS₂ (~162.9eV). Meanwhile, the valence state of Zn is investigated by X-ray absorption near edge spectroscopy (XANES) due to its insensitivity to XPS. The absorption edge of ZnS₂ shifts towards higher energy compared with bulk ZnS (Figure 3B), implying a higher valence state than +2. The unusual valence state originates from the unique structure of ZnS₂ monolayers, namely two S atoms equally share the electrons of a single Zn atom with an outer shell electron structure 3d¹⁰4s², make it impossible for sulfur atom to achieve octet stability. The Bader charge calculation (Figure 3C) and projected density of states (PDOS) also confirm that d-orbital electrons in Zn ion partially contribute to the Zn-S bonding, which leading to a higher valence state than Zn²⁺ in ZnS (Figures S28-S29).

Due to the unique electron-insufficient property of ZnS₂ monolayers, unsaturated atoms may serve as active sites to catalyze reactions. Considering the presence of lone-pair electrons in nitrogen molecules, we propose that the electron deficient ZnS₂ monolayers are efficient in

capturing and activating N₂ molecules, thus the electrocatalytic N₂ reduction reaction (NRR) is selected as a proof-of-concept experiment to test the catalytic properties of ZnS₂ monolayer. Quantification of NRR is conducted in a typical H-type cell in 0.1M KOH aqueous solution. As shown in Figure 4A, cyclic voltammetry curves show that a distinct reduction peak is observed in N₂ purged electrolyte, while there is no reduction peak in Ar purged electrolyte. As the applied potential changed, the ammonia yields, Faradic efficiencies (FE) and partial current density reach the peak at -0.3V vs. RHE, up to 27.3 µg/h/cm², 15.7% and 0.053 mA/cm² respectively (Figure 4B and Figure S30). The ammonia selectivity is comparable with state-of-the-art catalysts reported in literature (Table S3). Meanwhile, the HER reaction, which is considered as the typical side reaction during NRR are also quantified simultaneously via gas chromatography (GC) connected to the H-cell, the result in Figure 4C shows that as the potential gradually reaches to -0.3V vs. RHE, the corresponding HER reactions are significantly prohibited. To confirm the origin of high efficiency, 2D MoS₂ and FeS₂ are synthesized and tested under the same conditions as shown in Figure S31. The highest FE and NH₃ yield of MoS₂ and FeS₂ are close to 3.5%, 5.4 µg/h/cm² and 3.6%, 4.7 µg/h/cm², respectively (Figure S32). It's noted that the FeS₂ shows the similar valence states of cation and anion while the atomic structure is different, while MoS₂ shows similar structure but different valence states. These results further prove that electron deficient ZnS₂ can improve the NRR performance. The ZnS₂ catalyst also shows superior working stability according to the nearly proportional increase of ammonia concentration with the total amount of injected charge (Figure 4D) and highly stable catalysis current during the long-term reaction (Figure 4E). To exclude the illusion caused by the environment or contaminations a series of control experiments including ¹⁵N₂ isotope (Figure 4E insert) and OCV test are carried out (Figures S33-S36). The result is further evidenced by in-situ infrared (IR) spectroscopy (Figure 4F). Under the

constant bias (-0.3V vs. RHE), the peak at 1622cm⁻¹, which arises from the asymmetric δas (NH₃) bending vibrations of Lewis-bound NH₃ species³¹, shows remarkable increase as time elapsed. Moreover, the N-H stretch vibration at 3300cm⁻¹ and NH₂ rocking vibration³² at 1140cm⁻¹ also show increased intensities during NRR (Figure S37-38). These results indicated that the accumulation of NH₃ product is originated from the continuously reduction of N₂.

The N₂ chemical adsorption on catalyst plays a critical role in NRR, because intensive N₂ adsorption could weaken the triple bond in N₂ and promote the subsequent reaction. To probe the N₂ adsorption on ZnS₂, we employed an ambient pressure X-ray photoelectron spectroscopy (AP-XPS) which allows the direct injection of N₂ into sample chamber. Figure 5A-5C shows the changes of N 1s, Zn 2p and S 2p spectra of ZnS₂, respectively, as the N₂ pressure varies from UHV to 10 Pa. Under the UHV condition, no nitrogen-related signal can be detected. As the N2 pressure gradually increases to 1e⁻³ Pa and 0.1 Pa, a weak but distinguishable peak appears at 403 eV, suggesting the chemical adsorption of N₂ on ZnS₂ monolayer (Figure 5A). Further increase in the N₂ pressure to 10 Pa leads to an intensive peak around 407 eV, corresponding to the nitrogen molecules in gas phase. Meanwhile, both Zn 2p and S 2p shift to lower binding energy after the adsorption of N₂, indicating that the unoccupied electron orbitals in the catalyst interact with the lone-pair electrons from N₂ (Figure 5B-5C). In contrast, when injecting N₂ to the ZnS powder under the same condition, neither distinct chemical adsorption peak of N2 nor binding energy shift of catalyst are observed (Figure 5D-5F), indicating the very weak intrinsic adsorption of N₂. The DFT calculation also confirmed that nitrogen molecules can be stably adsorbed on freestanding monolayer ZnS₂ surface with a binding energy of -0.0996eV (Figure 5G), while the 2H-ZnS surface show weak bonding of N2, with a binding energy as low as -0.0157eV. As mentioned above, both Zn and S in ZnS₂ are electron-deficient, therefore they interact with the lone-pair electrons in nitrogen molecule, causing the enhanced chemical coupling of N₂.

Conclusion

In conclusion, we predict a new type of 2D metal dichalcogenides with d¹⁰s² electronic structure and produce ZnS₂ monolayers via metal-confined growth. The ZnS₂ monolayers possess an unusual 1-T atomic structure and electron-deficient ions, resultantly, they show excellent capability on nitrogen capture and reduction. As well, we expect the promising application this dichalcogenides in electronic, magnetic, optical, and catalytic fields because of their unique atomic and electronic structures. Our findings will stimulate theoretical and experimental research on the novel dichalcogenides that do not naturally exist.

AUTHOR INFORMATION

Corresponding Author

Xi-Wen Du*, <u>xwdu@tju.edu.cn</u>, Huolin L. Xin*, <u>huolin.xin@uci.edu</u> and Jun Luo*, <u>jluo@tjut.edu.cn</u>,

Author Contributions

The manuscript was written through contributions of all authors. X.W.D designed the project. R.Z., H.L.X., and X.W.D conceived the experiments and wrote the manuscript with input from all authors. R.Z., X.H.L. and H.L. developed method to prepare materials and conducted the basic characterization (SEM, XRD, XPS, AFM). C.Q.C., D.Y.W. and C.K.D. conducted the DFT calculation. R.Z., Q.J.G., J.M., J.M.Z., T.L., L.L.H. and J.L. prepared the FIB sample and

performed atomic-resolution S/TEM imaging and simulation. X.L.Z. conducted the EXAFS measurement. R.Z. and H.B.W. conducted the electrochemical measurement. A.H. conducted the AP-XPS experiment. R.Z. and X.T. conducted the atomic resolution STM imaging. Z.X.L. prepared the electrode and conducted the in-situ IR test.

Notes

The authors declare no conflict of interest.

ASSOCIATED CONTENT

Supporting Information. The Supporting Information is available free of charge. The materials and methods including synthesis and characterization are included. The DFT phonon prediction, products at different synthesis conditions, detail characterization of Zn/ZnS₂ NSs (AFM, SEM, EDS, HAADF-STEM, EFTEM, XPS, SEAD, cross-section STEM), in-situ etching/heating process (OM, HAADF-STEM and SAED), detail characterization of ZnS₂ monolayer (AFM, HAADF, XPS, EDS, HAADF/BF-STEM simulations, STM, FT-EXAFS and fitting), DOS of ZnS₂ monolayer, and all the detail control experiments of N₂ reduction reaction are included in Supporting Information.

ACKNOWLEDGMENT

We thank Yu-Zhu Zhou and Yi-Ren Lu for the collaboration of developing new materials and thank Ran Li, Zhi-Qing Li and Qing Chen for the exploration of device. This work is supported in part by the Natural Science Foundation of China (NSFC) grant (Nos. 51871160, 51671141,

51471115). This research used resources of the Center for Functional Nanomaterials, which is a U.S. DOE Office of Science Facility, at Brookhaven National Laboratory under Contract No. DE-SC0012704.

REFERENCES

- 1. Chhowalla, M.; Shin, H. S.; Eda, G.; Li, L.-J.; Loh, K. P.; Zhang, H., The chemistry of two-dimensional layered transition metal dichalcogenide nanosheets. *Nature Chemistry* **2013**, *5* (4), 263-275.
- 2. Voiry, D.; Fullon, R.; Yang, J.; de Carvalho Castro e Silva, C.; Kappera, R.; Bozkurt, I.; Kaplan, D.; Lagos, M. J.; Batson, P. E.; Gupta, G.; Mohite, Aditya D.; Dong, L.; Er, D.; Shenoy, V. B.; Asefa, T.; Chhowalla, M., The role of electronic coupling between substrate and 2D MoS₂ nanosheets in electrocatalytic production of hydrogen. *Nature Materials* **2016**, *15* (9), 1003-1009.
- 3. Mak, K. F.; Shan, J., Photonics and optoelectronics of 2D semiconductor transition metal dichalcogenides. *Nature Photonics* **2016**, *10* (4), 216-226.
- 4. Yin, Z.; Li, H.; Li, H.; Jiang, L.; Shi, Y.; Sun, Y.; Lu, G.; Zhang, Q.; Chen, X.; Zhang, H., Single-layer MoS₂ phototransistors. *ACS Nano* **2012**, *6* (1), 74-80.
- 5. Shahzad, F.; Alhabeb, M.; Hatter, C. B.; Anasori, B.; Man Hong, S.; Koo, C. M.; Gogotsi, Y., Electromagnetic interference shielding with 2D transition metal carbides (MXenes). *Science* **2016**, *353* (6304), 1137-40.
- 6. Ugeda, M. M.; Bradley, A. J.; Shi, S.-F.; da Jornada, F. H.; Zhang, Y.; Qiu, D. Y.; Ruan, W.; Mo, S.-K.; Hussain, Z.; Shen, Z.-X.; Wang, F.; Louie, S. G.; Crommie, M. F., Giant bandgap renormalization and excitonic effects in a monolayer transition metal dichalcogenide semiconductor. *Nature Materials* **2014**, *13* (12), 1091-1095.

- 7. Bolar, S.; Shit, S.; Murmu, N. C.; Samanta, P.; Kuila, T., Activation strategy of MoS₂ as HER electrocatalyst through doping-induced lattice strain, band gap engineering, and active crystal plane design. *ACS Applied Materials & Interfaces* **2021**, *13* (1), 765-780.
- 8. Zhang, L.; Ji, X.; Ren, X.; Ma, Y.; Shi, X.; Tian, Z.; Asiri, A. M.; Chen, L.; Tang, B.; Sun, X., Electrochemical ammonia synthesis via nitrogen reduction reaction on a MoS₂ catalyst: theoretical and experimental studies. *Advanced Materials* **2018**, *30* (28), 1800191.
- 9. Li, F.; Chen, L.; Liu, H.; Wang, D.; Shi, C.; Pan, H., Enhanced N₂-fixation by engineering the edges of two-dimensional transition-metal disulfides. *The Journal of Physical Chemistry C* **2019**, *123* (36), 22221-22227.
- 10. Akinwande, D.; Huyghebaert, C.; Wang, C. H.; Serna, M. I.; Goossens, S.; Li, L. J.; Wong, H. P.; Koppens, F. H. L., Graphene and two-dimensional materials for silicon technology. *Nature* **2019**, *573* (7775), 507-518.
- 11. Munkhbat, B.; Yankovich, A. B.; Baranov, D. G.; Verre, R.; Olsson, E.; Shegai, T. O., Transition metal dichalcogenide metamaterials with atomic precision. *Nature Communications* **2020,** *11* (1), 4604.
- 12. Wang, L.; Hu, P.; Long, Y.; Liu, Z.; He, X., Recent advances in ternary two-dimensional materials: synthesis, properties and applications. *Journal of Materials Chemistry A* **2017**, *5* (44), 22855-22876.
- 13. Li, J.; Zhao, B.; Chen, P.; Wu, R.; Li, B.; Xia, Q.; Guo, G.; Luo, J.; Zang, K.; Zhang, Z.; Ma, H.; Sun, G.; Duan, X.; Duan, X., Synthesis of ultrathin metallic MTe₂ (M = V, Nb, Ta) single-crystalline nanoplates. *Advanced Materials* **2018**, *30* (36), 1801043.
- 14. Shivayogimath, A.; Thomsen, J. D.; Mackenzie, D. M. A.; Geisler, M.; Stan, R.-M.; Holt, A. J.; Bianchi, M.; Crovetto, A.; Whelan, P. R.; Carvalho, A.; Neto, A. H. C.; Hofmann, P.;

- Stenger, N.; Bøggild, P.; Booth, T. J., A universal approach for the synthesis of two-dimensional binary compounds. *Nature Communications* **2019**, *10* (1), 2957.
- 15. Tang, B.; Zhou, J.; Sun, P.; Wang, X.; Bai, L.; Dan, J.; Yang, J.; Zhou, K.; Zhao, X.; Pennycook, S. J.; Liu, Z., Phase-controlled synthesis of monolayer ternary telluride with a random local displacement of tellurium atoms. *Advanced Materials* **2019**, *31* (23), 1900862.
- 16. Zhao, Y.; Qiao, J.; Yu, P.; Hu, Z.; Lin, Z.; Lau, S. P.; Liu, Z.; Ji, W.; Chai, Y., Extraordinarily strong interlayer interaction in 2D layered PtS₂. *Advanced Materials* **2016**, *28* (12), 2399-2407.
- 17. Ataca, C.; Şahin, H.; Ciraci, S., Stable, single-layer MX₂ transition-metal oxides and dichalcogenides in a honeycomb-like structure. *The Journal of Physical Chemistry C* **2012**, *116* (16), 8983-8999.
- 18. Rasmussen, F. A.; Thygesen, K. S., Computational 2D materials database: electronic structure of transition-metal dichalcogenides and oxides. *The Journal of Physical Chemistry C* **2015**, *119* (23), 13169-13183.
- 19. Zhou, J.; Lin, J.; Huang, X.; Zhou, Y.; Chen, Y.; Xia, J.; Wang, H.; Xie, Y.; Yu, H.; Lei, J.; Wu, D.; Liu, F.; Fu, Q.; Zeng, Q.; Hsu, C. H.; Yang, C.; Lu, L.; Yu, T.; Shen, Z.; Lin, H.; Yakobson, B. I.; Liu, Q.; Suenaga, K.; Liu, G.; Liu, Z., A library of atomically thin metal chalcogenides. *Nature* **2018**, *556* (7701), 355-359.
- 20. Silberberg, M. S., *Principles of general chemistry*. McGraw-Hill Higher Education: 2007.
- 21. Singh, D., Basic concepts of inorganic chemistry. Pearson Education India: 2011.
- 22. Jensen, W. B., The Place of zinc, cadmium, and mercury in the periodic table. *Journal of Chemical Education* **2003**, *80* (8), 952.

- 23. Maeno, Y.; Hagino, K.; Ishiguro, T., Three related topics on the periodic tables of elements. *Foundations of Chemistry* **2021,** *23* (2), 201-214.
- 24. Barreca, D.; Gasparotto, A.; Maragno, C.; Tondello, E.; Sada, C., CVD of nanophasic (Zn, Cd)S thin films: from multi-layers to solid solutions. *Chemical Vapor Deposition* **2004**, *10* (4), 229-236.
- 25. Liu, J. Z.; Yan, P. X.; Yue, G. H.; Kong, L. B.; Zhuo, R. F.; Qu, D. M., Synthesis of doped ZnS one-dimensional nanostructures via chemical vapor deposition. *Materials Letters* **2006**, *60* (29), 3471-3476.
- 26. Hamad, S.; Cristol, S.; Catlow, C. R. A., Surface structures and crystal morphology of ZnS: computational study. *The Journal of Physical Chemistry B* **2002**, *106* (42), 11002-11008.
- 27. Huang, X.; Tang, S.; Mu, X.; Dai, Y.; Chen, G.; Zhou, Z.; Ruan, F.; Yang, Z.; Zheng, N., Freestanding palladium nanosheets with plasmonic and catalytic properties. *Nature Nanotechnology* **2011**, *6* (1), 28-32.
- 28. Cai, C.; Ma, Y.; Jeon, J.; Huang, F.; Jia, F.; Lai, S.; Xu, Z.; Wu, C.; Zhao, R.; Hao, Y.; Chen, Y.; Lee, S.; Wang, M., Epitaxial growth of large-grain NiSe films by solid-state reaction for high-responsivity photodetector arrays. *Advanced Materials* **2017**, *29* (17), 1606180.
- 29. Li, X.; Cai, W.; An, J.; Kim, S.; Nah, J.; Yang, D.; Piner, R.; Velamakanni, A.; Jung, I.; Tutuc, E.; Banerjee, S. K.; Colombo, L.; Ruoff, R. S., Large-area synthesis of high-quality and uniform graphene films on copper foils. *Science* **2009**, *324* (5932), 1312-4.
- 30. Addou, R.; Colombo, L.; Wallace, R. M., Surface defects on natural MoS₂. *ACS Applied Materials & Interfaces* **2015**, *7* (22), 11921-11929.

31. Bahrami, B.; Komvokis, V. G.; Singh, U. G.; Ziebarth, M. S.; Alexeev, O. S.; Amiridis, M. D., In situ FTIR characterization of NH₃ adsorption and reaction with O₂ and CO on Pdbased FCC emission control additives. *Applied Catalysis A: General* **2011**, 391 (1), 11-21.

32. Zeng, L.; Li, X.; Chen, S.; Wen, J.; Huang, W.; Chen, A., Unique hollow Ni–Fe@MoS₂ nanocubes with boosted electrocatalytic activity for N₂ reduction to NH₃. *Journal of Materials Chemistry A* **2020**, 8 (15), 7339-7349.

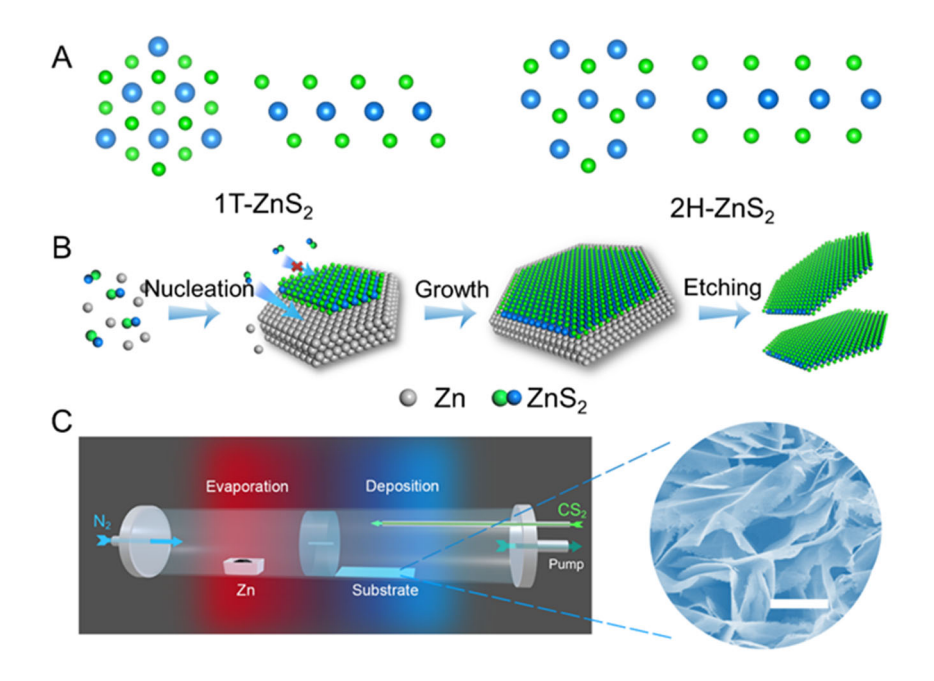


Figure 1. Prediction and synthesis of Zn metal dichalcogenides. (A) Prediction of potentially existed ZnS_2 with 1-T and 2-H phase (plane view and side view, respectively). (B) Schematic maps of nucleation, growth, and etching processes of sulfide/metal/sulfide sandwich structure in Zn-S system. (C) Experiment setup and the SEM image of the nanosheets with sandwich structure, scale bar 2 μ m.

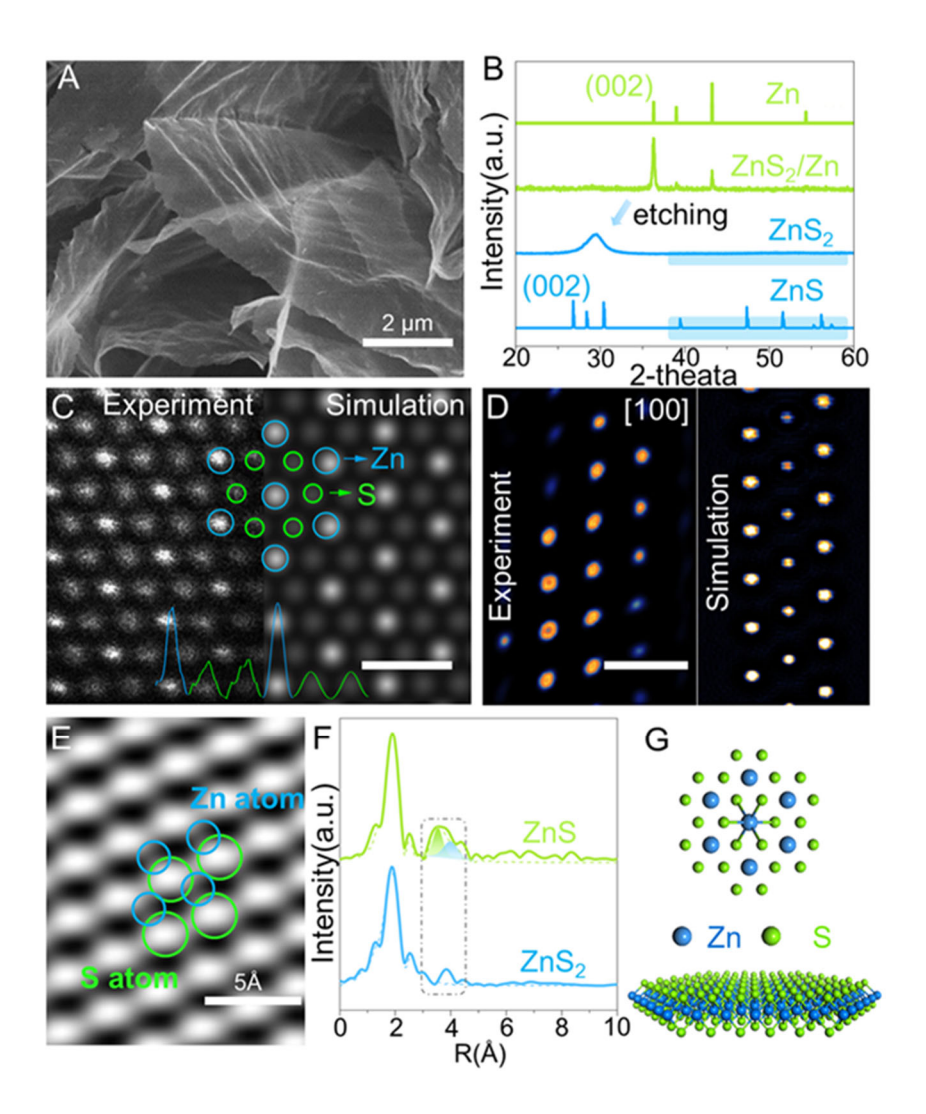


Figure 2. Characterizations of monolayer ZnS₂ structure. (A) SEM image of ultrathin ZnS₂ monolayers. (B) X-ray diffraction patterns of Zn@ZnS₂ nanosheets, monolayer ZnS₂, Zn powder and bulk ZnS. (C) HAADF-STEM image and simulated pattern of monolayer ZnS₂ in the plane view (blue: Zn; green: S, scalebar 5 Å). (D) AC-HRTEM image and simulated pattern of ZnS₂ in the side view, scale bar is 5 Å. (E) atomic resolution STM image of ZnS₂ surface. (F) Zn K-edge EXAFS spectra of monolayer ZnS₂ and bulk ZnS in R-space. (G) Atomic model of monolayer ZnS₂.

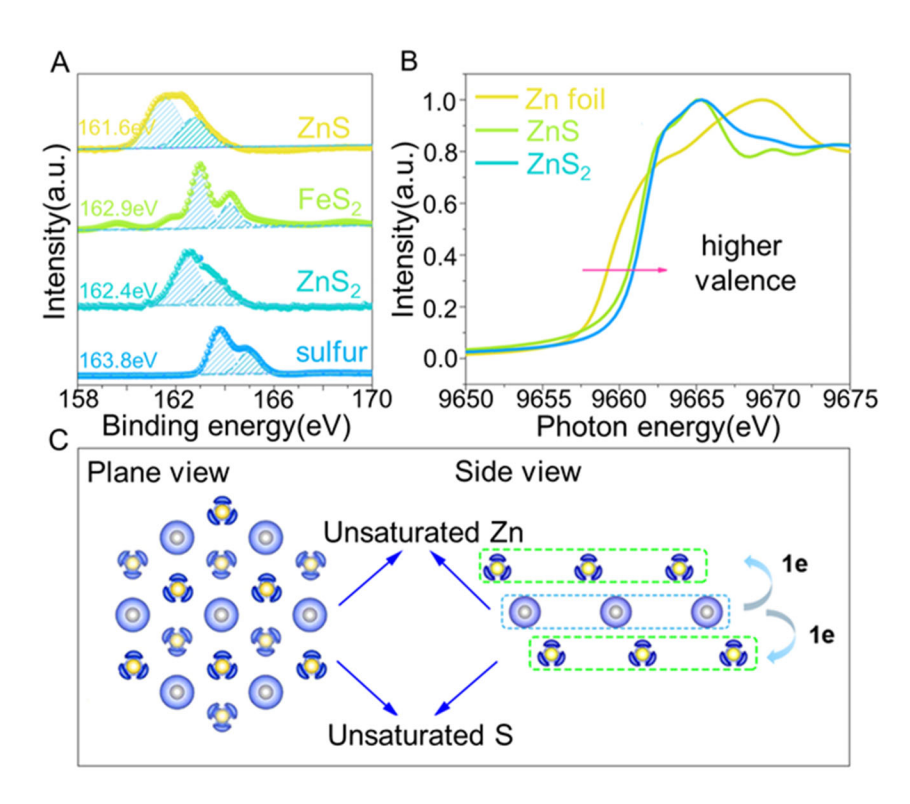


Figure 3. Valence states of monolayer ZnS₂. (A) XPS of S 2p in wurtzite ZnS, pyrite FeS₂, 1-T monolayer ZnS₂ and S powder. (B) Zn K-edge XANES of ZnS₂, wurtzite ZnS and metallic Zn. (C) Bader charges of the unsaturated sulfur and Zn atoms in monolayer ZnS₂.

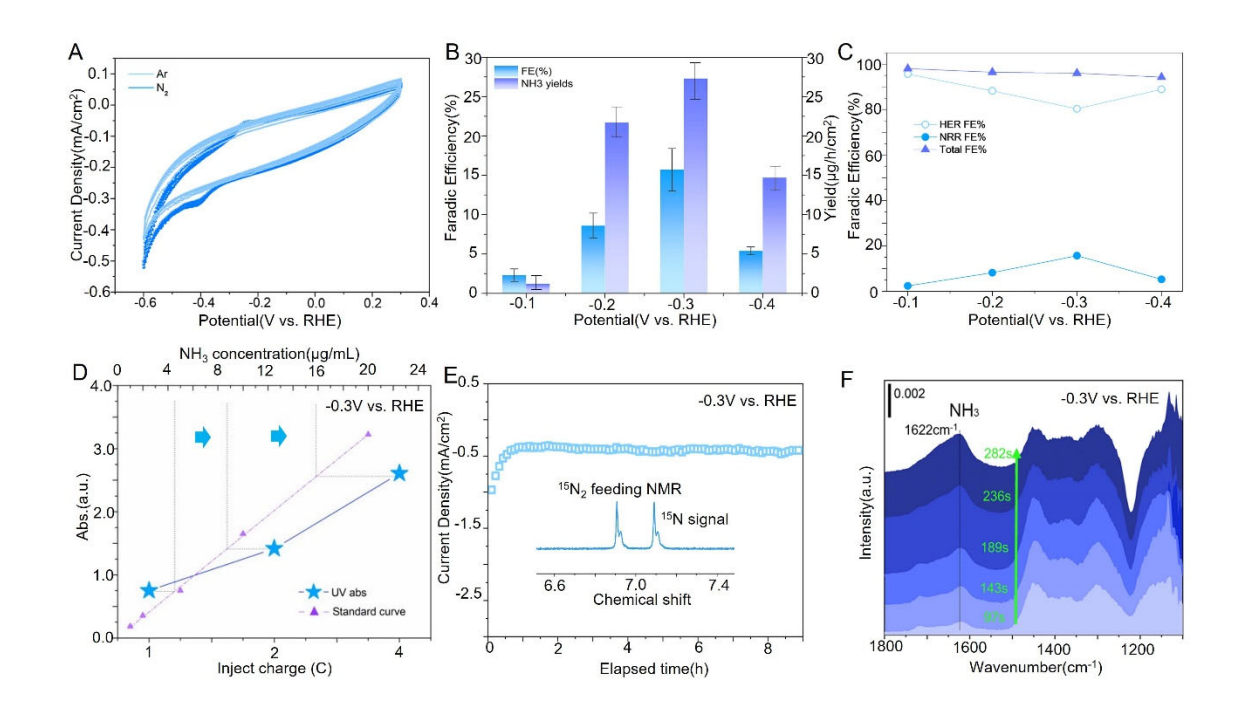


Figure 4. Catalytic properties of monolayer ZnS₂ for nitrogen reduction. (A) CV curves of ZnS₂ in Ar and N₂ purged 0.1M KOH. (B) NH₃ yield (violet) and Faradic efficiency (blue) at each given potential. (C) Simultaneously quantification of HER and NRR faradic efficiency. (D) The relationship of ammonia concentration with total injected charge. (E) I-T curve at -0.3V vs. RHE and the NMR result of product using ¹⁵N₂ as feeding gas. (F) Time elapsed IR at -0.3V (vs. RHE), the IR absorption intensity scale bar is 0.002.

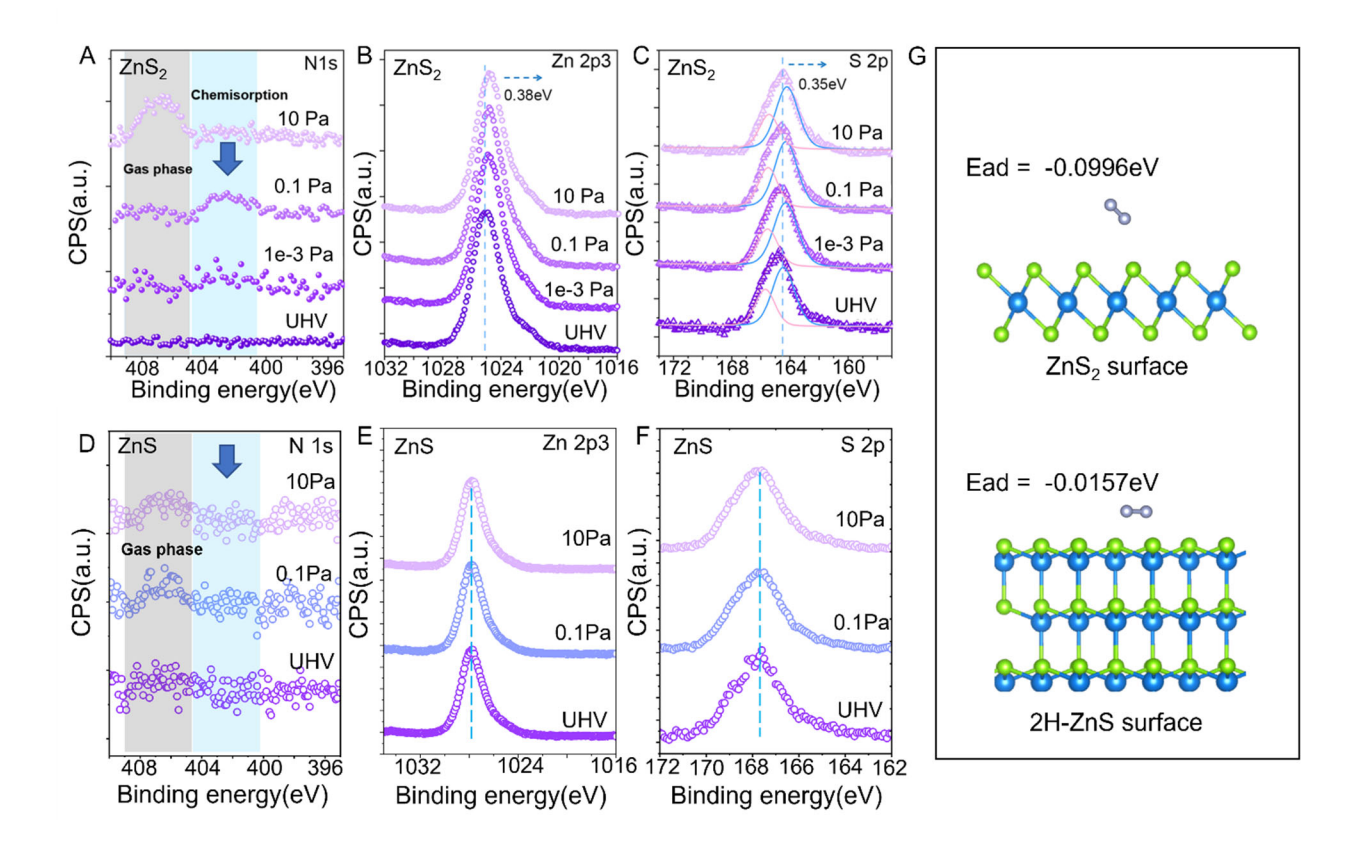


Figure 5. In-situ observation of N₂ adsorption on the surface using AP-XPS. (A) N 1s, (B) Zn 2p3, and (C) S 2p XPS spectra of ZnS₂ monolayer at different N₂ pressures. (D) N 1s, (E) Zn 2p3, and (F) S 2p XPS spectra of ZnS powder at different N₂ pressures. (G) N₂ adsorption energy on ZnS₂ surface and ZnS surface.

Table of Contents Entry

